

The APEX calibration plan: goals, implementation, and achievements

Michael Dumke and Felipe Mac-Auliffe

ESO, Alonso de Cordova 3107, Vitacura, Santiago, Chile

ABSTRACT

The quality of scientific data depends on the accuracy of the absolute intensity calibration. This absolute calibration is especially difficult in ground-based sub-mm astronomy. At the Atacama Pathfinder Experiment (APEX), we take various measures in order to ensure a proper calibration of the final science product, including real-time efforts (e.g. pointing models) and dedicated measurements whose results are applied afterwards (e.g. opacity or efficiencies). In this presentation we will give an overview over the various steps taken at APEX to overcome most calibration challenges. We will explain their implementation as calibration plan, present an analysis of the results obtained, and discuss those results in view of the reliability of the released science product.

Keywords: APEX telescope, Calibration, Bolometer, Opacity, Heterodyne receiver, Sideband ratio

1. INTRODUCTION

The usage of observational data to estimate physical conditions in astronomical objects has – as far as the calibration is concerned – two basic requirements. The data need to be calibrated, and the uncertainty in this calibration must be known quantitatively to the principal investigator (PI) of a science project. In radio astronomy, many different factors enter into the calibration. There are instrumental factors, like the absolute temperature scale, efficiencies, sideband ratios and such, as well as environmental factors, like atmospheric transmission and stability. In the sub-mm atmospheric window, which has just been opened during the last two decades for astronomical observations, latest receiver technologies are used, and the atmospheric absorption (and emission) plays a significant role in the data taking process. Thus for sub-mm observations these factors become even more important than for classical radio astronomy at longer wavelengths.

The Atacama Pathfinder EXperiment (APEX)^{1,2} is a modified ALMA prototype antenna, with 12 m diameter, used for frequencies between 200 GHz and 1.4 THz. APEX is currently equipped with two facility continuum receivers: The Large APEX Bolometer Camera (LABOCA)^{3,4} is a 295 channel bolometer array, for observations in the $\lambda 850 \mu\text{m}$ atmospheric window. The Submillimeter APEX Bolometer Camera (SABOCA)⁵ is a 37 channel TES bolometer array, for the $\lambda 350 \mu\text{m}$ atmospheric window. For spectral line observations, the Swedish Heterodyne Facility Instrument (SHFI)⁶ is available, with four single-pixel heterodyne receivers with central frequencies of 230, 345, 460, and 1300 GHz.

The APEX telescope is located at an altitude of 5100 m in the Chilean Altiplano, close to the desert village San Pedro de Atacama. Its location aims to minimize the environmental effects on the calibration, as well as the use of the latest technology aims to minimize the instrumental effects. Still these effects exist, and they need to be taken into account during observations and data reduction to obtain properly calibrated science data.

At APEX we take these effects into account by the implementation of a calibration plan. The ultimate goal of this plan is to optimize the absolute intensity calibration of the obtained science data, and to quantify the remaining calibration uncertainty. The efforts to ensure a good calibration and to quantify it can be divided into two phases. The first phase comprises the observations (and their preparation), where real-time measures are taken in order to obtain the best possible calibrated data. The second phase comprises the data reduction, when the data are going through various calibration steps. This second phase depends strongly on the type of observation (continuum or spectral line), since different calibration schemes are applied and therefore different

Further author information: (Send correspondence to M.D.)

M.D.: E-mail: mdumke@eso.org; F.M.: E-mail: fauliffe@eso.org

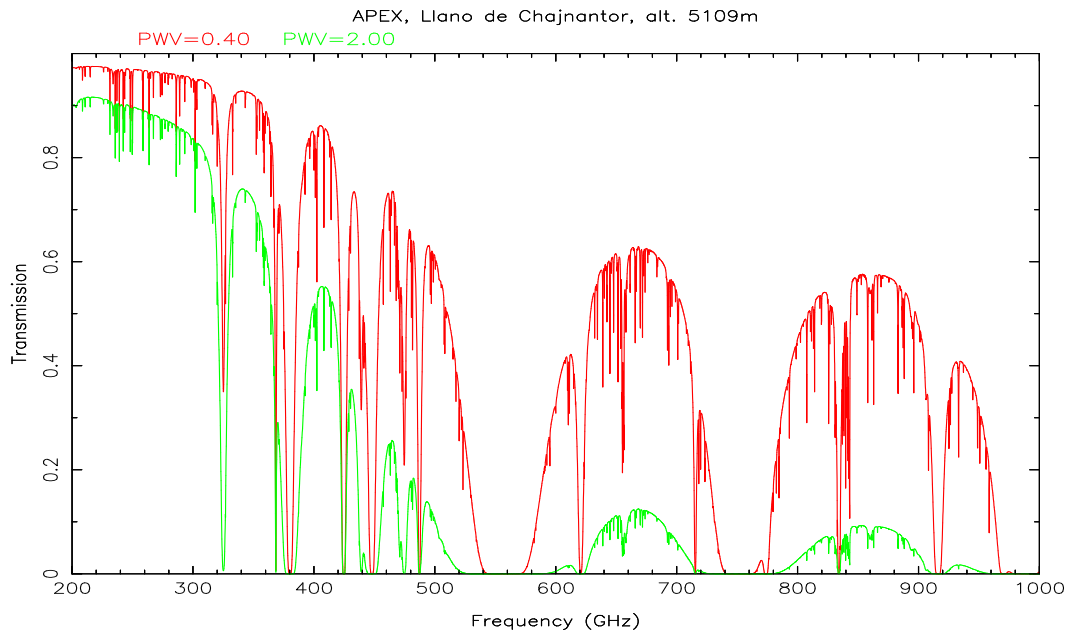


Figure 1. Atmospheric transmission as function of observing frequency at the APEX site on Chajnantor for 0.4 mm (dark grey, upper curve) and 2.0 mm (light grey, lower curve) of precipitable water vapor.

calibration measurements and procedures are required. Thus this paper is organized in the following way. In section 2 we will present the calibration efforts performed before or during the data taking process. Section 3 will describe the post-observation calibration efforts for continuum data, while section 4 will give an overview over the spectral line calibration. Both sections do not only describe the calibration, but also address the problem of the calibration uncertainty of the final data. Finally, in section 5 we will summarize the achievements obtained with the calibration plan implementation at APEX.

2. THE OBSERVING PROCESS

In order to obtain the best absolute calibration scale possible, first measures have to be taken during (or even before) the actual observing process.

2.1 Atmospheric conditions

The atmospheric transmission of the astronomical signal is a strong function of frequency. The most important limiting factor in the sub-mm range is absorption lines of water. The amount of gaseous water in the atmosphere above a certain location is known as precipitable water vapor (pwv), measured in mm. Fig. 1 illustrates this dependency.

With its facility receivers, APEX covers a frequency range between 200 GHz and almost 1.4 THz. It is therefore almost always possible to select the science project to be observed (and hence the receiver to be used) according to the current atmospheric conditions. The main selection is made based on the current value for the precipitable water vapor. Table 1 summarizes the selection criteria used by the APEX staff.

Until $pwv = 5$ mm, the atmospheric transmission at e.g. 230 GHz is still 80 %, which justifies observations with the APEX-1 receiver. If the water vapor rises to even higher values, there are usually other factors which prevent observations as well, like very strong winds or snowfall, thus at APEX we do not perform science observations if $pwv > 5$ mm.

Besides the absolute value of the water vapor, a number which is more important in terms of calibration is the variation in the water vapor. Some results are presented in Section 4.3.

Table 1. Facility receiver usage as function of the precipitable water vapor. Further information about the receivers is available on the APEX website.⁷

Receiver	APEX-1	APEX-2	APEX-3	APEX-T2	LABOCA	SABOCA
Frequency [GHz]	211–275	275–370	385–500	1250-1390	345	850
Recommended water vapor [mm]	1.5-5.0	0.8-2.5	0.2-1.0	< 0.2	0.5-2.0	< 0.6

2.2 Positional accuracy and pointing models

An exact positioning of the telescope is vital for observations of point sources and sources with spatially changing physical properties.

The absolute position of the telescope is measured by a set of optical encoders in Azimuth and Elevation with an angular resolution of $0''.02$. The astronomical position where a certain receiver is looking at differs from this because of several influences: telescope tilts, deformations of the dish, feed legs, and backup structure, alignment accuracy of the various mirrors in the optical path, receiver offset from the optical axis, etc. These differences are described by a pointing model which is automatically loaded into the system to correct for these differences.

A basic pointing model is regularly obtained on stars with an optical telescope mounted off-axis behind the primary mirror. The use of stars (compared to radio sources) has the advantage that several hundred sources can be observed within a few hours of observing time to obtain a good estimate of the second and third order terms in the pointing model.

APEX uses a model with a total of 28 free parameters. Many of them are telescope "constants", thus they are fitted using data collected through several pointing sessions. Only a few parameters are expected to vary from one pointing run to the next, or from one receiver to another. They can be obtained on a dedicated pointing session with a given receiver. The procedure to obtain a pointing model is described in somewhat more detail elsewhere in this volume.⁸

The uncertainties of this pointing model represent the main error in the telescope positioning. The residual positioning error of the pointing model, dependent on various factors (availability of pointing sources, atmospheric conditions) varies around $2''-3''$, independent of the actual receiver. Since the pointing accuracy is also constantly verified on strong point sources during an observing run, the actual average positioning error is estimated to be about $1''.5$.

In Table 2, we have summarized the expected intensity losses (calculated from the beam size) when observing a point source with a telescope positioning error between $1''$ and $3''$. Obviously, the intensity loss is more severe for higher frequencies and the corresponding smaller beam sizes. Another limiting factor for the pointing accuracy at high frequency is the fact that the number of strong point sources to allow a pointing check does decrease with frequency.

The facility bolometers (LABOCA, SABOCA) are not as much affected, since the default observing mode is mapping. Thus a pointing error may result in a position error in the final map, but not in an intensity loss. This is not true for the recently commissioned photometric mode for the APEX bolometers.

2.3 Focusing of the telescope

Besides the positional accuracy, also the proper focusing of the telescope has a significant effect on the absolute calibration.

The focus is adjusted by moving the secondary mirror (subreflector), which is mounted on a hexapod that gives the necessary degrees of freedom for these movements. The subreflector can be moved along three axes (x , y , and z , which correspond to azimuth, elevation, and along the optical axis, respectively) and tilted around two axes (x , y). A tilt around the z axis would not make sense since it translates into a pure rotation of the subreflector, which does not change anything because of the subreflector's symmetry.

In praxis the tilts have been determined during the commissioning of the telescope and have been constant since. The translations along the axes are measured and corrected, if necessary, on a strong pointing source at the beginning of each observing session and whenever the focus is expected to change, mainly because of temperature changes (i.e. after sunrise or sunset, or when changing the illumination (by sunlight) of the telescope structure).

Table 2. Point source intensity loss for various positioning errors.

Frequency [GHz]	230	345	460	850	1300
Receiver	APEX-1	APEX-2, LABOCA	APEX-3	SABOCA	APEX-T2
<i>HPBW</i>	27''	18''	13''5	7''3	4''8
Intensity loss for a positioning error of					
1''0	0.4 %	0.9 %	1.5 %	5.1 %	11 %
1''5	0.9 %	1.9 %	3.4 %	11 %	24 %
2''0	1.5 %	3.4 %	5.9 %	19 %	38 %
3''0	3.4 %	7.4 %	13 %	37 %	66 %

Thus the absolute focusing error is usually kept < 0.2 mm, which translates to intensity losses of < 1 % to a few percent, depending on frequency.

2.4 Additional factors

Overall it should be mentioned that the factors described here are not only valid for APEX. All radio telescopes encounter similar challenges. In comparison with other telescopes, and given the excellent pointing and focus accuracy, we conclude that these factors do not affect the absolute calibration. This is not true when comparing data at different frequencies. Because of the factors described in this section and their semi-statistical nature, we would expect a systematic underestimate of line intensities at high frequencies, with negligible effects below 500 GHz, but rather considerable effects above 1 THz. These effects are not taken into account for the delivered science data product. It remains the PI's task during post-processing.

3. CONTINUUM CALIBRATION

The calibration of bolometer observations consists of two parts: instrument calibration and atmosphere (astronomical) calibration. In this section we will mainly refer to LABOCA, since the calibration procedures for SABOCA are still under development, due to the limited amount of data available up to now.

3.1 Array parameters

During observations with multichannel bolometer arrays, the target source is covered by a large fraction (maybe all) of the individual bolometers in the array, leading to a large number of separate maps of the area of interest. During the data reduction process, these maps are shifted according to their location in the array, and corrected for their individual gains. These parameters – location and gain – need to be known very exactly in order to produce a combined map without artefacts.

In order to obtain these array parameters, a strong, compact continuum source (ideally Mars, Uranus, or Neptune) is observed in On-the-Fly mapping mode, with a map size large enough to cover the source with all individual bolometers of the array. A dedicated reduction routine does a two-dimensional Gaussian fit on the individual maps, and the fit results yield the positional offsets (relative to the nominal location of the channel in the array) and the relative gain of the channel. Fig. 2 shows the obtained channel locations within the array for LABOCA (left) and SABOCA (right). In order to obtain a sufficient S/N for these parameters, several parameter sets, obtained during periods without major maintenance work on the corresponding bolometer array, are averaged.

For the final array parameters, the average positional uncertainty of the individual channels is $0''.7$ for LABOCA and $0''.4$ for SABOCA. The effect of this uncertainty is similar to the effect of adding up various maps with some pointing error (i.e. an increase of the effective beam size), but much smaller, and therefore negligible.

The average error of the individual channel gains is about 3 % for LABOCA and 7 % for SABOCA. However, since some channels may overestimate the intensity, and others underestimate it, they cancel each other out to a certain extent. The remaining calibration error is again negligible compared to those introduced by the absolute calibration process, which is explained in the following subsections.

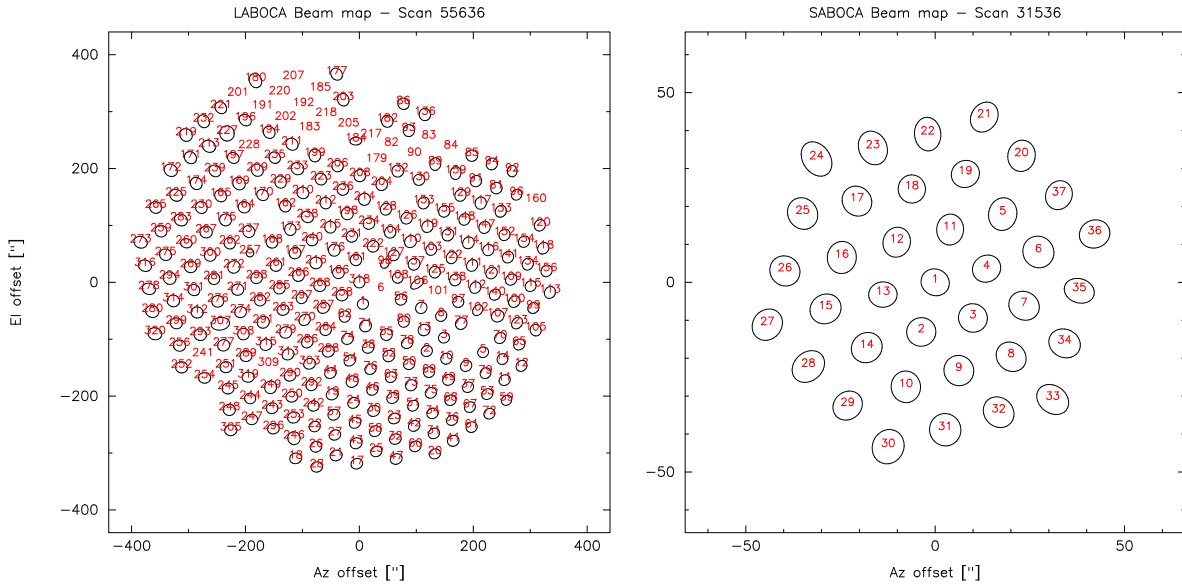


Figure 2. The positions of the individual channels of LABOCA (left) and SABOCA (right) within the bolometer array, as obtained by a fully sampled planet map covering the source with all channels. Note the different scale for the two bolometer arrays.

3.2 Sky opacities

The atmospheric transmission for astronomical radiation can be described by

$$I_{\text{rec}} \sim I_0 e^{-\tau_z \sec z} \quad (1)$$

with the received intensity I_{rec} , the intensity outside the atmosphere I_0 , the zenith opacity τ_z and the zenith angle $z = 90^\circ - El$. This formula does not take into account Earth's curvature, but is sufficiently accurate for elevations above 25° , where almost all science observations are carried out. While the elevation is given by the telescope position, the zenith opacity has to be measured.

At APEX, we apply a two-step process to estimate zenith opacities. The first is a so-called skydip measurement, where the actual receiver (LABOCA or SABOCA) is used. During a continuous scan from $El = 82^\circ$ down to $El \sim 23^\circ$ (this value may vary depending on the actual conditions), the atmospheric emission is measured and its dependence on the elevation fitted by a model.

The second step are continuous measurements of the precipitable water vapor in the atmosphere using a radiometer which is sensitive around a water absorption line at 183 GHz. This radiometer is installed in the Cassegrain cabin of the telescope, thus it measures the same line-of-sight through the atmosphere towards the target. It uses three different IFs in order to sample the center and two different frequencies in the wings of the absorption line. Based on the ratio of the intensities measured in the different IFs, the precipitable water vapor (and therefore the opacity) is calculated. It should be noted that this method becomes somewhat unreliable for very small values of pvw (< 0.4 mm), when the absorption in the line wings becomes very small.

The usage of these two independent measurements resulted from our experience during the first two years of LABOCA operation. It was figured out that the opacities fitted from the skydips using the facility Bolometer Data Analysis Software (BoA)⁹, τ_{sd} , are consistently lower than the numbers from radiometer measurements. In order to obtain an agreement between observed and expected primary calibrator fluxes, an average opacity of $1.3\tau_{\text{sd}}$ needs to be applied to the data. The reason for this discrepancy is that the BoA software uses the ambient temperature as best guess for the atmosphere temperature in the fitting process. Attempts to treat the atmosphere temperature as free parameter during the fitting process led to unrealistic high values for the opacity. Thus the BoA developers decided to fix this number (F. Schuller, priv. comm.).

Table 3. Secondary calibrators for continuum observations, their positions, and flux density values at $\lambda 870 \mu\text{m}$.

Source	HL Tau	CRL618	V883 Ori	N2071IR	VY CMa	CW Leo	B13134
RA[J2000]	04:31:38.45	04:42:53.60	05:38:18.24	05:47:04.85	07:22:58.33	09:47:57.38	13:16:43.15
Dec[J2000]	18:13:59.0	36:06:53.7	-07:02:26.2	00:21:47.1	-25:46:03.2	13:16:43.6	-62:58:31.6
$S_{870\mu\text{m}}$	2.0 ± 0.2	4.8 ± 0.5	1.4 ± 0.3	9.1 ± 0.8	1.5 ± 0.2	4.1 ± 0.3	12.9 ± 1.3
Source	IRAS16293	G5.89	G10.62	G34.3	G45.1	K3-50A	CRL2688
RA[J2000]	16:32:22.90	18:00:30.37	18:10:28.66	18:53:18.50	19:13:22.07	20:01:45.69	21:02:18.80
Dec[J2000]	-24:28:35.6	-24:04:01.4	-19:55:49.7	01:14:58.6	10:50:53.4	33:32:43.5	36:41:37.7
$S_{870\mu\text{m}}$	16.1 ± 1.3	27.6 ± 0.2	33.0 ± 1.8	55.3 ± 3.7	8.0 ± 0.6	14.7 ± 1.4	5.5 ± 0.9

Similarly it was found that the opacity calculated from radiometer measurements (τ_{rm}) needs to be corrected by a factor of 0.9 to yield on average a good agreement between observed and expected primary calibrator fluxes. Thus the reference opacity for a given skydip scan is calculated as the average: $\tau_{\text{ref}} = 0.5(1.37\tau_{\text{sd}} + 0.9\tau_{\text{rm}})$.

This reference opacity still contains a significant level of uncertainty, which we address by regular observations of primary and secondary calibrators during an observing run.

3.3 Primary and secondary calibrators

During a normal observing run, primary calibrators (Mars, Uranus, Neptune) as well as secondary calibrators (see Table 3) are observed in regular intervals. The flux densities of the planets can be well predicted based on models, taking into account distance, diameter, and illumination (phase). In practice they are estimated using the Astro program of the Gildas Software¹⁰. The flux density scale of the secondary calibrators is then estimated relative to the primary calibrators, with the relation mentioned in the previous subsection for the sky opacities. We are currently also investigating the use of asteroids as potential calibrators for LABOCA and SABOCA.

The main secondary calibrators used for continuum flux calibration are summarized together with their flux densities at $\lambda 870 \mu\text{m}$ in Table 3. Because of the amount of SABOCA data being much less, the APEX staff is still in the process of estimating the flux densities at $\lambda 350 \mu\text{m}$.

During every observing session with the bolometers, calibrators are observed regularly. Their measured flux density is corrected for the sky opacity by a linear interpolation of the reference opacities of the skydips observed closest in time. By comparison of this corrected flux density with the expected flux density (Table 3 for LABOCA) a correction factor is calibrated and can be applied to the target source flux density scale, if necessary. With these correction factors obtained by calibrator measurements, all systematic errors in the opacity calculation by skydips can be corrected for. The standard deviation for these correction factors is $\sigma(f_{\text{CalCorr}}) = 0.14$ and $\sigma(f_{\text{CalCorr}}) = 0.35$ for LABOCA and SABOCA, respectively. These numbers correspond to the scatter of the calibrator fluxes (and hence also of the science data) *before* these correction factors are applied to the data. A better estimate for the calibration uncertainty *after* these correction factors have been applied can be obtained when only calibrator scans over a few hours (the typical uninterrupted daily observing time of a given project) are considered. The resulting standard deviations of the calibrator correction factors are 0.05 and 0.24 for LABOCA and SABOCA, respectively, translating to relative calibration uncertainties of 5% and 24%. For LABOCA, this number is of the same order as the flux density uncertainty of the secondary calibrators themselves. Thus we estimate an absolute calibration uncertainty of 10% for LABOCA. For SABOCA currently the absolute calibration uncertainty is 25 – 30%.

We should close this subsection with the comment that we recently found a dependence of the correction factor introduced here on the precipitable water vapor. We are working on an understanding of this effect and will take it into account during future improvements of the calibration scheme.

3.4 Further calibration issues with broadband bolometers

Both facility bolometers are broadband instruments, and the spectral response is mainly defined by a set of filters. LABOCA is sensitive between 300 and 400 GHz, SABOCA between 700 and 1000 GHz. This wide bandpass has several consequences.

- **Beam size.** Over such a wide bandpass, the beam size (angular resolution) changes significantly. The half-power beam width for LABOCA is $HPBW \sim 16'' - 20''$, and for SABOCA $HPBW \sim 6''.5 - 8''.5$, while all bolometer maps are calibrated in e.g. mJy/beam with a median beam size. For extended sources, the detected flux originates in a larger area (in the source) for emission at the lower end of the bandpass than for emission at the upper end. Depending on the spectral energy distribution (SED) of the source, an over- or underestimate of the measured flux may occur.
- **Effective frequency.** The amount of atmospheric absorption changes over the band. For excellent weather this change is small, but for higher p_{wv} the absorption towards the higher end of the bandpass is significantly higher than towards the lower end (see Fig. 1). Thus the effective observing frequency will decrease. Besides a change in beam size (see above), this also changes the actual flux density, depending on the slope of the source SED. This effect may be more severe if the target source SED differs significantly from the SED of the used calibrators over the bolometer bandpass.

While these consequences have effects on the calibration, it is not yet known how severe they are. They are generally assumed to be rather small compared to the overall calibration uncertainty. We are currently in the process of investigating these effects for the APEX bolometers.

4. SPECTRAL LINE CALIBRATION

The calibration efforts for spectral line data can be divided in two phases. The first phase includes the actual calibration of the data, as it is performed by the Online Calibrator software described in the next subsection. After that step the data product is delivered to the project PIs. With additional information about telescope efficiencies the calibration scale can be adjusted to be telescope-independent. At this stage, the data can be used for scientific research and – in a perfect world – should be perfectly calibrated.

In practice this is not necessarily the case. In the second phase, results from an APEX calibration monitoring program can be taken into account. The goal of this program is to verify the absolute calibration scale, to detect deviations, and to estimate absolute calibration uncertainties inherent to the data. This monitoring program consists of regular observations of well known molecular line sources, the standardized reduction and analysis of the resulting data, and the comparison of the results between various dates and with results available from other observatories or in publications. This monitoring program has only been implemented for APEX-1 and APEX-2 yet. The APEX-3 receiver has just recently been installed, and for the APEX-T2 receiver, the observations of calibration sources will be performed within the science projects, because it would require a large amount of excellent weather time otherwise.

The first phase will be covered in Sections 4.1 and 4.2, the second phase in the remainder of this section.

4.1 The Online Calibrator

The absolute calibration of spectral line data is based on receiver noise temperatures and system temperatures estimated by so-called SKY-HOT-COLD calibration scans which are performed immediately before the actual spectral line observations. In this section we outline the basic steps performed by the software, a detailed description of the calibration concept is available elsewhere^{11,12}.

During the three phases of a calibration scan, the receiver is looking during equal amounts of time to blank sky, to a hot load at ambient temperature, and to a cold load at liquid nitrogen temperature. From these data, the Online Calibrator calculates first the receiver temperature T_{rec} from the signal in the HOT and COLD phases. Then it proceeds and calculates the sky temperature T_{sky} by taking into account the SKY signal, and correcting for spillover and forward efficiency F_{eff} (see section 4.2).

From the elevation of the SKY measurement, it calculates the airmass, based on a curved atmosphere, which is used by the ATM modul to determine the opacity in image and signal band, with the aid of a sophisticated atmospheric model. As a final step in the calibration scan reduction, the calibration temperature T_{cal} and system temperature T_{sys} are calculated and stored internally.

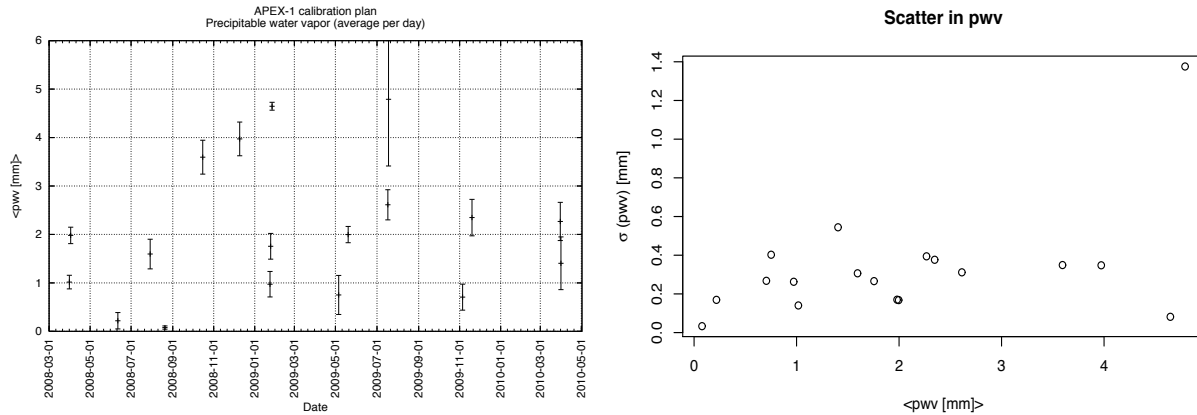


Figure 3. **a.** (left panel) Averaged precipitable water vapor for all dates when monitoring observations were performed with the APEX-1 receiver. **b.** (right panel) Standard deviation of the averaged p_{wv} as function of p_{wv} . There is no obvious dependency of $\sigma(p_{wv})$ on $\langle p_{wv} \rangle$.

The following spectral line scans are then calibrated via

$$T_A^* = (C_{\text{on}} - C_{\text{off}})G^{-1}T_{\text{cal}} \quad (2)$$

with C_{on} and C_{off} being the signals (counts) in the ON and OFF phase of the spectral line scan, G the gain (calculated before from the calibration scan, and T_A^* the antenna temperature, corrected for F_{eff} and rear spillover. At this stage the data are considered calibrated, and are delivered to the PI. This calibration, however, is telescope specific.

4.2 Efficiencies

The spectral line data, as it is delivered to the PI, is calibrated in T_A^* . In order to obtain a telescope-independent calibration, this temperature scale must be converted to e.g. main beam brightness temperature, T_{mb} . In the calibration scheme used at APEX, these temperature scales are connected via $T_{\text{mb}} = (F_{\text{eff}}/B_{\text{eff}})T_A^*$, with the forward efficiency F_{eff} and the main beam efficiency B_{eff} . The forward efficiency is defined as the radiation received from the forward direction relative to the radiation received from all directions. For standard radio telescopes, this number is slightly smaller than, but close to, unity. The value which is applied by default at APEX is $F_{\text{eff}} = 0.95$, although recent measurements suggest values of 0.97 and 0.96 for APEX-1 and APEX-2, respectively.

Similarly, the main beam efficiency B_{eff} is the radiation received from the main beam relative to the radiation received from all directions. This number depends on the beam pattern of the telescope and therefore on e.g. the surface accuracy. It also depends on the beam filling factor and is therefore – strictly speaking – only correct for point sources. It can be measured by continuum scans on planets. By measurements performed during 2008 using Mars, Jupiter, and Saturn, we found a main beam efficiency of $B_{\text{eff}} = 0.80$ for 230 GHz, and 0.74 at 345 GHz. It depends also on the observing frequency, and decreases towards higher frequencies.

4.3 Observing conditions

As already introduced in subsection 2.1, the receiver to be used during science observations (and hence the observing frequency) is normally selected based on the precipitable water vapor (p_{wv}) present in the atmosphere. However, also the actual variation in p_{wv} has to be taken into account in this decision. An example of the effect of a strongly varying p_{wv} can be seen in Fig. 4a.: for almost all dates the scatter in the data points is comparable, except for one (2009-07-19). At that particular date not only the averaged absolute value for p_{wv} was rather high, but also its standard deviation (which basically means its variability). The p_{wv} as function of date, as well as the standard deviation $\sigma(p_{wv})$ as function of p_{wv} , are shown in Fig. 3.

Table 4. Relative calibration uncertainty for various frequencies.

Molecule	APEX-1	H ₂ CO	¹³ CO	CO	CH ₃ OH	CS	HCN				
ν [GHz]	all	218.2	220.4	230.5	241.8	244.9	265.9				
Spectra	345	30	58	122	21	70	44				
σ_I	0.083	0.057	0.100	0.058	0.097	0.089	0.131				
σ_T	0.079	0.072	0.076	0.076	0.100	0.078	0.087				
Molecule	APEX-2	CS	OCS	C ¹⁸ O	¹³ CO	CH ₃ OH	CS	CO	HCN	HCO ⁺	H ₂ CO
ν [GHz]	all	293.9	304.1	329.3	330.6	338.4	342.9	345.8	354.5	356.7	362.7
Spectra	577	43	46	37	136	20	36	147	41	43	28
σ_I	0.141	0.106	0.135	0.134	0.139	0.330	0.151	0.082	0.140	0.113	0.243
σ_T	0.113	0.078	0.094	0.119	0.131	0.236	0.096	0.082	0.103	0.082	0.160

The calibration uncertainty is therefore not so much a function of the absolute water vapor value (which is calibrated out by the Online Calibrator), but rather of the variability of the water vapor on the timescale relevant for the calibration. This timescale is given by the frequency of HOT-SKY calibration measurements (every 10 to 15 minutes). This is demonstrated by the data from 2009-01-27, with a water vapor of 4.65 ± 0.09 mm (see Fig. 3), where no strong variation in the calibration is seen. A low absolute pvw value means less atmospheric transmission, and therefore higher signal-to-noise ratios, and will also result in smaller opacity correction factors (i.e. less amplification of any kind of noise or scatter). But also the stability of the atmospheric conditions is important for a reliable calibration. For bolometer observations this is even more crucial, because the subtraction of correlated atmospheric noise between the individual bolometer channels becomes more difficult or even impossible at the presence of short-term atmospheric instabilities.

4.4 Calibration uncertainty

A good estimate for the calibration stability and uncertainty can be obtained by calculating normalized line parameters for the spectral lines observed within our calibration plan monitoring program. These parameters are basically the maximum brightness temperature T_{\max} and the velocity integrated line intensity $I = \int_{\text{line}} T dv$ (sometimes also nominated line area). While the first is more uncertain in the presence of spikes, the latter shows a higher dependence on the spectral baseline. It is therefore expected to show a larger variation for weak sources.

To obtain normalized parameters, reference spectra are created from all observations performed during the monitoring program by averaging the spectra for each source/line combination with an appropriate weighting for all observation dates. The normalized line parameter (T or I) is then simply the actual value divided by the parameter obtained from the average spectrum.

Analysing T_{\max} and I for all sources and lines, we find the following standard deviations for the normalized parameters: $\sigma(T_{\max}) = 0.079$ and $\sigma(I) = 0.083$ for the APEX-1 receiver, and $\sigma(T_{\max}) = 0.113$ and $\sigma(I) = 0.141$ for the APEX-2 receiver. If we assume that the average project PI is able to perform a proper baseline subtraction for his science data, then we can estimate the overall calibration uncertainty to 8% and 12% for the APEX-1 and APEX-2 receiver, respectively. However, this uncertainty strongly depends on the actual source and/or line; it is much lower for the “standard” lines (CO(2–1) and CO(3–2)) than for others.

Table 4 summarizes all numbers for both receivers. For lines which are monitored in LSB and USB tuning we averaged the numbers, since the differences (for the normalized parameters!) have been found to be negligible. While for the APEX-1 receiver the calibration uncertainty is $\leq 10\%$ for all lines, for APEX-2 there are higher values for some cases. These are C¹⁸O(3–2) and ¹³CO(3–2), with an uncertainty of about 13%, and even more H₂CO and CH₃OH with an uncertainty of up to $\sigma_I = 33\%$ for the latter. The reason for this large scatter at these special frequencies is currently unknown. A possible explanation could be a tuning instability, with a strongly varying image band rejection. Further dedicated tests need to be performed to investigate this situation.

4.5 LSB vs. USB tuning

In general any frequency (except close to the edges of the tuning range) can be observed in lower sideband (LSB) and upper sideband (USB) tuning. Ideally, both tunings should give very similar results. For a total of five lines

Table 5. USB/LSB sideband response ratios for various frequencies

Molecular line	CO(2-1)	CS(5-4)	OCS	13CO(3-2)	CO(3-2)
Frequency [GHz]	230.5	244.9	304.1	330.6	345.8
$I_{\text{USB}}/I_{\text{LSB}}$	0.97 ± 0.04	0.99 ± 0.05	0.96 ± 0.04	0.91 ± 0.06	0.90 ± 0.04

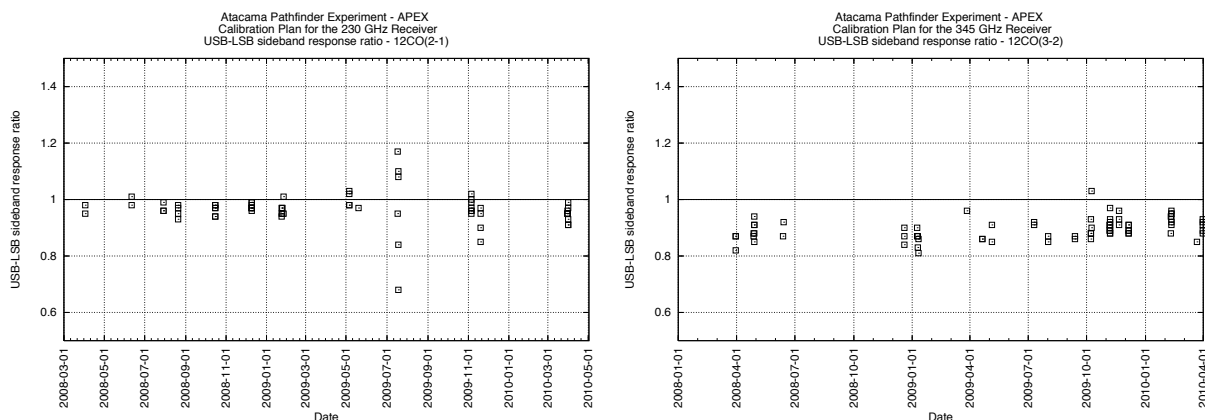


Figure 4. The USB vs. LSB sideband response ratio for the CO(2-1) and the CO(3-2) line, the most important molecular transitions for the APEX-1 and APEX-2 receiver, respectively. For both lines USB intensities are smaller than LSB intensities. Note also the large scatter for date 2009-07-19 for the CO(2-1) line (see Section 4.3).

(two with APEX-1, three with APEX-2) we monitor line parameters using both tunings.

A comparison of the two different tunings is possible by calculating the sideband response ratio $I_{\text{USB}}/I_{\text{LSB}}$, the ratio of the line intensities when observed with upper and lower sideband tuning (not to be confused with the “sideband ratio”, which is the ratio of signal to image band for *one* tuning). The sideband response ratio is listed for the five lines in Table 5. We find that USB tuning always results in lower intensities than LSB tuning. While this is not very significant for APEX-1, the differences are clear for APEX-2, especially for CO(3-2), which is the standard molecular line for this receiver. Fig. 4 illustrates the effect for APEX-1 and APEX-2, and also shows that this ratio does not vary significantly with time.

This result is independent of the precipitable water vapor during the observations. Thus it does not seem to be affected by differences in the atmospheric transmission between the sidebands. It rather seems that the image sideband rejection differs from the numbers which are assumed by the Online Calibrator (see Section 4.1). As we will see in Section 4.6, the spectra obtained in USB tuning seem to be in better agreement with data from other telescopes, while the line intensities obtained in LSB tuning seem to be too large. Thus the sideband rejection for LSB tuning seems to be better than assumed by the Online Calibrator.

We should note here that an improvement of the calibrator software is under discussion, e.g. by implementing a channel dependent calibration, rather than an averaged one over the whole band. Also, a better determination of the image band rejection, by line injection at the frequencies of the signal and image band for various tunings, and the application of these improved numbers in the calibrator, may improve the sideband calibration accuracy in the future.

4.6 Comparison with other telescopes

We compared the reference spectra obtained with the APEX-1 and APEX-2 receiver with data from other telescopes, to verify if the overall absolute calibration scales are consistent. This comparison was restricted to point-like or very compact sources, in order to properly correct for the varying beam dilutions as result of different telescope diameters (i.e. beam sizes). An extensive database is available online for the JCMT¹³, as well as for other telescopes (CSO, SEST) through published articles^{14,15,16}.

The comparison was performed for the following sources: CRL618, OH231.8, IRC+10216, IRAS15194, and CRL2866. IRC+10216 is known to be extended for the CO(2-1) and (3-2), as well as the 13CO(2-1) transition,

but at rather low intensity levels. We treated the correction for beam dilution as if it was a point source. The inclusion or non-inclusion of these transitions in the data analysis does not change the final results described in this subsection.

The results differ depending on which APEX receiver is considered (APEX-1 or APEX-2), and also on the telescope the comparison data come from. For APEX-2, the APEX data are in good agreement with JCMT and CSO, with an average peak brightness temperature ratio of $\langle T_{\text{JCMT+CSO}}/T_{\text{APEX2}} \rangle = 1.02 \pm 0.12$. Given the larger number of comparison spectra available at JCMT, we can separate data taken at APEX with LSB tuning from USB tuning, and find $\langle T_{\text{JCMT}}/T_{\text{APEX2,LSB}} \rangle = 0.97 \pm 0.14$ and $\langle T_{\text{JCMT}}/T_{\text{APEX2,USB}} \rangle = 1.00 \pm 0.13$, respectively. While the ratios are within the uncertainty in all cases, there is apparently a trend to overestimate brightness temperatures when using LSB tuning with the APEX-2 receiver. The difference found by comparison with JCMT data is consistent with the overall trend seen in Section 4.5, that USB tuning in general gives lower brightness temperatures than LSB tuning. We can therefore summarize that data obtained in USB tuning using the APEX-2 receiver are fully consistent with comparison data taken at other telescopes, while data taken with the same receiver in LSB tuning seem to overestimate the line temperatures.

For APEX-1, the situation is different. Separating the two sideband tunings for the APEX-1 receiver and taking into account only JCMT comparison data, we find $\langle T_{\text{JCMT}}/T_{\text{APEX1,LSB}} \rangle = 0.86 \pm 0.18$ and $\langle T_{\text{JCMT}}/T_{\text{APEX1,USB}} \rangle = 0.87 \pm 0.13$ for LSB and USB tuning, respectively. If we included SEST data, the numbers would be even slightly lower (with an average of $\langle T_{\text{JCMT+SEST}}/T_{\text{APEX1}} \rangle = 0.84 \pm 0.10$), but SEST data were known to slightly underestimate brightness temperatures in general (A. Lundgren, priv. comm.). Still there remains a discrepancy between APEX data taken with the APEX-1 receiver and JCMT data. These results do not claim neither that JCMT intensities are too low nor that APEX intensities are too high, still APEX project PIs should be aware of these calibration differences. Again, comparing with Section 4.5 it looks like the results using USB tuning with the APEX-1 receiver seem to be in better agreement than those from LSB tuning, although the difference is smaller than for the APEX-2 receiver.

5. SUMMARY AND CONCLUSIONS

In this paper we presented the efforts undertaken at APEX to obtain the best possible absolute intensity calibration for the science data product which is delivered to the end user (the PI). We introduced the various steps taken at (or even before) the observations until the reduction pipeline, and estimated the uncertainties introduced already in the observation process, like pointing and focusing error.

For bolometer observations, the array parameters can be estimated very accurately and their errors are negligible. The main uncertainty for calibration comes from the opacity determination. At APEX, we use a method based on skydips and radiometer measurements to minimize the errors. In addition, regular calibrator observations are used to further reduce the remaining uncertainty, which is estimated to 10% for LABOCA observations and 25% for SABOCA observations.

For heterodyne data we found that the calibration scale at APEX is in very good (APEX-2) to moderate (APEX-1) agreement with other telescopes, and estimated the calibration uncertainty to 8% and 12% for APEX-1 and APEX-2, respectively. For the latter a discrepancy between LSB and USB tuning has been found, and the USB numbers seem to be more reliable.

Based on the findings presented here, we will continue to improve the calibration methods in the future to obtain an even lower absolute calibration uncertainty for APEX data. Especially for SABOCA data we are working on a flux density scale for secondary calibrators, as well as on an improved opacity determination, in order to reduce the errors. As a courtesy to the user, the APEX staff maintains a set of webpages where the calibration information for LABOCA¹⁷ and the results from the SHFI monitoring program¹⁸ are available.

Acknowledgements. We would like to thank all APEX staff and partner institute astronomers who have carried out calibration observations throughout the years, as well as Giorgio Siringo and Axel Weiß for their valuable input about bolometer calibration. We acknowledge the use of gnuplot¹⁹ and R²⁰ for some data analysis and plotting purposes.

REFERENCES

- [1] Güsten, R., Nyman, L. Å., Schilke, P., Menten, K., Cesarsky, C., and Booth, R., “The Atacama Pathfinder EXperiment (APEX) - A new submillimeter facility for southern skies -,” *Astron. Astrophys.* **454**, L13–L16 (2006).
- [2] Güsten, R., Booth, R. S., Cesarsky, C., Menten, K. M., Agurto, C., Anciaux, M., Azagra, F., Belitsky, V., Belloche, A., Bergman, P., De Breuck, C., Comito, C., Dumke, M., Duran, C., Esch, W., Fluxa, J., Greve, A., Hafok, H., Häupl, W., Helldner, L., Henseler, A., Heyminck, S., Johansson, L. E., Kasemann, C., Klein, B., Korn, A., Kreysa, E., Kurz, R., Lapkin, I., Leurini, S., Lis, D., Lundgren, A., Mac-Auliffe, F., Martinez, M., Melnick, J., Morris, D., Muders, D., Nyman, L. A., Olberg, M., Olivares, R., Pantaleev, M., Patel, N., Pausch, K., Philipp, S. D., Philipps, S., Sridharan, T. K., Polehampton, E., Reveret, V., Risacher, C., Roa, M., Sauer, P., Schilke, P., Santana, J., Schneider, G., Sepulveda, J., Siringo, G., Spyromilio, J., Stenvers, K., van der Tak, F., Torres, D., Vanzì, L., Vassilev, V., Weiss, A., Willmeroth, K., Wunsch, A., and Wyrowski, F., “APEX: the Atacama Pathfinder EXperiment,” *Proc. SPIE* **6267** (2006).
- [3] Siringo, G., Kreysa, E., Kovacs, A., Schuller, F., Weiß, A., Esch, W., Gemünd, H., Jethava, N., Lundershausen, G., Güsten, R., Menten, K. M., Beelen, A., Bertoldi, F., Beeman, J. W., Haller, E. E., and Colin, A., “The large APEX bolometer camera LABOCA,” *Proc. SPIE* **7020** (2008).
- [4] Siringo, G., Kreysa, E., Kovács, A., Schuller, F., Weiß, A., Esch, W., Gemünd, H.-P., Jethava, N., Lundershausen, G., Colin, A., Güsten, R., Menten, K. M., Beelen, A., Bertoldi, F., Beeman, J. W., and Haller, E. E., “The Large APEX BOLometer CAMera LABOCA,” *Astron. Astrophys.* **497**, 945–962 (2009).
- [5] Siringo, G., Kreysa, E., De Breuck, C., Kovacs, A., Lundgren, A., Schuller, F., Stanke, T., Weiss, A., Guesten, R., Jethava, N., May, T., Menten, K. M., Meyer, H., Starkloff, M., and Zakosarenko, V., “A New Facility Receiver on APEX: The Submillimetre APEX Bolometer Camera, SABOCA,” *The Messenger* **139**, 20–23 (2010).
- [6] Vassilev, V., Meledin, D., Lapkin, I., Belitsky, V., Nyström, O., Henke, D., Pavolotsky, A., Monje, R., Risacher, C., Olberg, M., Strandberg, M., Sundin, E., Fredrixon, M., Ferm, S.-E., Desmaris, V., Dochev, D., Pantaleev, M., Bergman, P., and Olofsson, H., “A Swedish heterodyne facility instrument for the APEX telescope,” *Astron. Astrophys.* **490**, 1157–1163 (2008).
- [7] “APEX Instrumentation.” <http://www.apex-telescope.org/instruments>.
- [8] Lundgren, A., Rabanus, D., Güsten, R., Menten, K. M., de Zeeuw, T., Olofsson, H., Kaufer, A., Nyman, L. A., Bergman, P., De Breuck, C., Wyrowski, F., Agurto, C., Azagra, F., Dumke, M., Mac-Auliffe, F., Martinez, M., Montenegro, F., Muders, D., Reveret, V., Risacher, C., Parra, R., Siringo, G., and Wieching, G., “APEX: Five Years of Operations,” *Proc. SPIE* **7737** (2010).
- [9] “Bolometer array analysis software.” <http://www.astro.uni-bonn.de/boawiki/>.
- [10] “GILDAS - Grenoble Image and Line Data Analysis Software.” <http://www.iram.fr/IRAMFR/GILDAS>.
- [11] Kutner, M. L. and Ulich, B. L., “Recommendations for calibration of millimeter-wavelength spectral line data,” *Astrophys. J.* **250**, 341–348 (1981).
- [12] Mangum, J., “Amplitude Calibration at Millimeter and Submillimeter Wavelengths,” *ALMA Memo No. 318* (2000). <http://www.alma.nrao.edu/memos/html-memos/abstracts/abs318.html>.
- [13] “Representative Spectra for the JCMT Heterodyne Receivers.” Website, available under the URL: http://www.jach.hawaii.edu/JCMT/spectral_line/Standards/spectra_new.html.
- [14] Stanek, K. Z., Knapp, G. R., Young, K., and Phillips, T. G., “Maps of the Molecular Emission around 18 Evolved Stars,” *Astrophys. Journal Suppl. Ser.* **100**, 169 (1995).
- [15] Wang, Y., Jaffe, D. T., Graf, U. U., and Evans, II, N. J., “Single-sideband calibration for CO, (13)CO, HCN, and CS lines near 345 GHz,” *Astrophys. Journal Suppl. Ser.* **95**, 503–515 (1994).
- [16] Woods, P. M., Schöier, F. L., Nyman, L., and Olofsson, H., “Molecular abundances in carbon-rich circumstellar envelopes,” *Astron. Astrophys.* **402**, 617–634 (2003).
- [17] “LABOCA calibration.” <http://www.apex-telescope.org/bolometer/laboca/calibration>.
- [18] “The SHFI Calibration Plan.” <http://www.apex-telescope.org/heterodyne/shfi/calibration>.
- [19] “Gnuplot - a portable Graphing Utility.” <http://www.gnuplot.info>.
- [20] “The R Project for Statistical Computing.” <http://www.r-project.org>.